Applied Physics A (2020)126:904
https://doi.org/10.1007/s00339-020-04091-3

Applied Physics A
Materials Science & Processing

A novel method for graphene synthesis via electrochemical process and its utilization in organic photovoltaic devices

Kuray Dericiler[1] · Hamed Moeini Alishah[2] · Sinem Bozar[2] · Serap Güneş[2] · Figen Kaya[3]

Received: 7 July 2020 / Accepted: 18 October 2020
© Springer-Verlag GmbH Germany, part of Springer Nature 2020

Abstract
Graphene nanosheets have been prepared from fine graphite powders by a novel electrochemical exfoliation method using non-volatile sulfate salts. This new method utilizes a stainless steel wire cage and platinum wire electrodes to exfoliate pre-pelleted graphite powders into graphene sheets. Synthesized graphene samples have been characterized by Field Emission Scanning Electron Microscopy (FE-SEM), Raman spectroscopy, and Fourier Transform Infrared (FT-IR) spectroscopy. The obtained supernatant shows a stable suspension in DMF. This suspension was then used in organic solar cells (OSCs) as an additive to poly(3,4-ethylene dioxythiophene) polystyrene sulfonate (PEDOT:PSS). Organic solar cells have been prepared using Indium Tin Oxide (ITO) as the transparent conducting oxide, PEDOT:PSS-Graphene as the hole transport layer (HTL), Poly(3-hexylthiophene-2,5-diyl:[6,6]-Phenyl-C60-butyric acid methyl ester (P3HT:PCBM) as the active layer and Aluminum as the cathode, in ITO/PEDOT:PSS-Graphene/P3HT:PCBM/Al configuration. The photovoltaic cell prepared with graphene as an additive inside PEDOT:PSS exhibited over 66% improvement compared to the reference cells employing pure PEDOT:PSS.

Keywords Graphene · Electrochemical · Synthesis · Organic · Solar · Photovoltaic

1 Introduction

Graphene, thanks to its unique 2D hexagonal honeycomb lattice structure comprising carbon atoms making sp^2 hybridization, shows great mechanical strength of ~ 1100 GPa, very high intrinsic carrier mobility of ~ 200,000 cm^2/Vs, excellent thermal conductivity of ~ 5000 W/mK, near-perfect transparency in visible light (~ 97.7%) and consequently attracted the interest of numerous researchers since its discovery in 2004 by Andre Geim and Konstantin Novoselov [1–3]. This variety of astonishing features resulted in various areas of application for graphene, involving but not limited to liquid crystal device electrodes [4], pseudocapacitors [5], catalysis [6], transistors [7], electrochemical and biosensors [8], polymer electrolyte membrane (PEM) and direct methanol fuel cells (DMFC) [9, 10], batteries [11, 12], transmission electron microscopy sample supports [13], hydrogen storage [14] and photovoltaic devices [15–18].

To this day, many methods have been developed to synthesize graphene that possesses the exceptional properties stated above. Chemical vapor deposition (CVD) [19], unzipping of carbon nanotubes [20], gas-driven exfoliation [21, 22], oxidation followed by chemical or thermal reduction [23–25], and also other exfoliation techniques such as microwave exfoliation [26], shear exfoliation [27], sonochemical exfoliation [28], micromechanical exfoliation [1] and electrochemical exfoliation [29] have been developed over the years. While all these methods have advantages and disadvantages to each other, CVD, oxidation and subsequent reduction, and electrochemical exfoliation methods seem most promising among them. Chemical vapor deposition is the technique in which carbon atoms are deposited onto a suitable substrate, forming perfectly ordered single-layer graphene sheets, however, the technique itself is quite

✉ Kuray Dericiler
kuraydericiler@sabanciuniv.edu

[1] Department of Materials Science and Nano Engineering, Faculty of Engineering and Natural Sciences, Sabancı University, 34956 Tuzla, İstanbul, Turkey

[2] Department of Physics, Davutpasa Campus, Faculty of Arts and Science, Yıldız Technical University, 34210 Esenler, İstanbul, Turkey

[3] Department of Metallurgical and Materials Engineering, Davutpasa Campus, Faculty of Chemistry and Metallurgy, Yıldız Technical University, 34210 Esenler, İstanbul, Turkey

Published online: 30 October 2020

expensive because of the high end and costly equipment as well as highly-trained staff requirements. Although the end-product has an excellent quality, it is safe to assume that this method, unless there is a significant breakthrough, is not suitable for large-scale or automated production of graphene. The Oxidation–reduction method is a great alternative offering cheap and scalable production, nevertheless, the final product is generally structurally defected and/or contain Oxygen-containing impurities. Among the three, electrochemical exfoliation is found to offer the best of the two worlds, such as structurally intact and impurity-free yield with great scalability aspects [30].

Electrochemically exfoliating graphitic precursors to graphene is carried out essentially in two main approaches, namely anodic exfoliation, and cathodic exfoliation. In cathodic exfoliation, the electrode that is expected to exfoliate (graphite) is subjected to negative bias voltages, whereas in anodic exfoliation a positive voltage is applied to the active electrode, while both in the presence of an appropriate electrolyte. It is found that certain sodium-, alkylammonium-, imidazolium- and lithium-based salts in organic solvents such as propylene carbonate (PC) [31], acetonitrile [32], dimethyl sulfoxide (DMSO) [33], or N,N-dimethylformamide (DMF) [34] to be efficient towards this end. The mechanism of the cathodic exfoliation process is suggested as the intercalation of the cations that are formed in the electrolytes subsequent to the bias voltage. In the case of $LiClO_4$ in PC, these cations are $(Li{\cdot}2PC)^+$ and $(Li{\cdot}3PC)^+$ [31]. Although the process is carried out under reducing conditions, therefore, avoids the excess oxidation of electrode and also the end-product, resulting in greater structural quality and lower oxygen contents [33–35], main drawbacks such as long process times (several hours) followed by similarly long sonication treatment in a proper solvent to complete sheet separation of the cathodically intercalated product [36]. Furthermore, in order to upscale the process, it is required to use large amounts of these organic solvents which are not desirable from an environmental standpoint and also the high boiling point some of the solvents can be an issue for the subsequent processes of the products. Anodic exfoliation, on the other hand, can be easily accomplished in aqueous mediums with short intercalation times using appropriate intercalating anions from widely available chemicals such as acids (e.g., H_2SO_4) [37], their inorganic salts [Na_2SO_4, K_2SO_4, $(NH_4)_2SO_4$)] [38, 39], or ionic liquids [40] that readily separate to anions and cations, as electrolytes. The driving force of this process is described by Lu et al. as (I) oxidation of water near the anode, creating $(OH)^-$ and O^{-2} radicals, (II) hydroxylation or oxidation of edge planes, opening the edge sheets for intercalating anion to get in between the sheets, (III) expansion of the graphite anode due to intercalation and polarization of sheets and (IV) precipitation of exfoliated sheets in the solution [41].

In organic solar cells (OSCs), to simply put, organic material in the active layer of the cell absorbs photons coming from the sun, exciting electrons to create electron–hole pairs. These electrons and holes are then collected at the respective electrodes to generate electrical current. Nowadays, bulk heterojunctions (BHJs) are widely investigated [42]. However, direct contact between active layer materials and electrodes causes current leakage driven recombination, lowering overall cell efficiency. To minimize the effect of recombination, functional layers at the electrode/active layer interface are required in order to support charge extraction, and subsequent collection. These supporting layers, however, must be selective enough to filter a specific type of charge (hole or electron) and block the other one. Currently, p-type materials with a wide bandgap and high level of work function (WF) are used to block the electron and make ohmic contact with donor polymer [43]. Aside from certain metal oxides such as MoO_3, V_2O_5, NiO, Cu_2O [44, 45], poly(3,4-ethylenedioxithiophene) (PEDOT) doped with poly(styrene sulfonic acid) (PSS). (PEDOT:PSS) is one of the widely investigated and the most well-known transparent conducting oxide, which contributes a lot to the organic semiconductor devices. Its optical transparency at visible range, tunable electrical conductivity and work function, high flexibility and stretchability are the indispensable advantages that the researchers stick on this material [46] and it is almost considered the default hole transport material for solution-processed organic semiconductor devices. However, there are disadvantages of PEDOT:PSS, which include acidity, hygroscopicity, anisotropic charge injection and batch-to-batch variation in electrical and physical properties [47]. Therefore, there has been much research into developing materials to replace PEDOT:PSS and address the mentioned problems such as CuSCN [48], and NiO [49] including metal oxides such as V_2O_5, and WO_3 [50]. However, the majority of these HTLs rely on vacuum processing and/or complex chemistries that require high-temperature annealing, which in turn makes the overall cell manufacturing more complex and energy-intense. On the other hand, tremendous effort has been spent to modify PEDOT:PSS. In this respect, two research strategies stood out, one of which is focused directly on the replacement of the PEDOT:PSS with another counterpart to get rid of its disadvantages, and the other strategy is the modification of PEDOT:PSS. Among these two research strategies modification of PEDOT:PSS is highly preferred. Because, although slightly higher efficiencies may be achieved through replacement strategies the major draw back is the more complex and energy intensive production techniques of the materials used as a replacer. Lin et al. used solution processed, liquid exfoliated WS_2 layers as a replacement of PEDOT:PSS. They achieved a 17% of power conversion efficiency (PCE) [51]. However, they have achieved a PCE of 16.4% using

PEDOT:PSS as a hole transporter with the same active layer combination. Although they have achieved a slightly higher PCE, the exfoliation of WS_2 layer may be more complex as compared to that PEDOT:PSS is processed through single step spin coating procedure. As summarized above, although there are several drawbacks for the use of PEDOT:PSS, its modification with other counterparts to overcome the disadvantages such as degradation, acidity and hygroscopicity and etc. found significant research response and our motivation was to contribute to this research response by modifying PEDOT:PSS with graphene to improve the disadvantages of PEDOT:PSS and thereby improve the device performance. For this purpose, we synthesized graphene from powder-like graphitic precursors in such a way that it delivers high-quality products while maintaining a high yield and utilized electrochemically synthesized graphenes as an additive to PEDOT:PSS to increase the overall efficiency of the cell. In this scope, we used a steel wire cage and mild sonication to further assist the exfoliation of graphite which would normally break off and fall to the bottom of the beaker. Herein we report the electrochemical synthesis of graphene and its utilization as an additive to PEDOT:PSS to form HTL in an OSC.

There have been some reports about utilizing graphene oxides synthesized with modified Hummer's method [15, 52, 53], graphene oxide with similar composites [54] or graphene quantum dots (GQDs) [18] as HTLs but to the best of our knowledge, this is the first report on the utilization of the steel wire cage method and also the first report on the utilization of electrochemically synthesized graphene-PEDOT:PSS composite in organic solar cells as a hole transport layer.

2 Materials and methods

Fine graphite powders (Extra pure, Merck) were first pressed into pellets using a hand press (Newport, Premere). Typically, 1 g graphite powder was pressed into a pellet with a pressure of ~ 222 MPa. This pellet was later used as a graphitic precursor. 0.1 M 100 mL Na_2SO_4 (99%, Merck) aqueous solution was used as the electrolyte. Stainless steel wire cage (1810 CrNi, Commercial) was placed on the beaker while wetting the bottom part of the mesh. A Pt wire (99.5%) was submerged in the solution and acted as the cathode while the other was then placed on the mesh and acted as anode with the graphite pellet that was on top of it. The whole system was then placed in an ultrasonic cleaning bath (Kudos SK1200H, 45 W) to apply mild sonication. A bias voltage of + 10 V and sonication applied to the system at the same time. The goal here was to initially expand/exfoliate the graphite pellet, using a Pt wire and the pellet itself as the anode, then to prevent non-exfoliated sheets from settling on the bottom of the beaker using mild sonication, reintroduce them to the anode to properly exfoliate. As the pellet exfoliates and breaks apart, stainless steel mesh and nearby non-exfoliated graphite become the anode. The process was kept running until the pellet was completely disappeared and then 60 more minutes before termination, in order to minimize the amount of non-exfoliated graphite. The as-exfoliated product was collected, washed copiously with DI water (Elga Purelab Flex) via vacuum filtration using 0.2 µm pore sized PTFE membrane (ISOLAB) and dried in the oven at 80 °C overnight. Half of the dried powder kept further for analysis while the other half was redispersed in DMF (99.8%, Merck) via mild sonication. The product is then centrifuged at 4000 rpm in order to separate large-sized particles that are not exfoliated. The supernatant of the suspension decanted for further use. All experiments in this section were done at room temperature. Figure 1 illustrates the design of the experiment setup.

In order to prepare organic solar cells, subsequent layers have been created first. ITO coated glass with a thickness around 120 nm, a sheet resistance of 12 Ω/sq. and a size of 1.5×1.5 cm^2 (Kintec LTD) were used as anode transparent conductive electrode. One-third of ITOs was patterned by etching with an acid mixture ($HCl:HNO_3:H_2O$) and then each substrate was cleaned with distilled water, acetone, and isopropanol in an ultrasonic bath for 20 min, respectively. The aqueous solution of PEDOT:PSS (CLEVIOS™ PH 1000) filtered with a 0.45 µm Whatman filter. HTL has been prepared by mixing PEDOT:PSS with graphene suspension with a volumetric ratio of 5:1 PEDOT:PSS to graphene. The prepared solution was then spin-coated onto ITO coated glass first at 2000 rpm for 50 s. After annealing at 140 °C

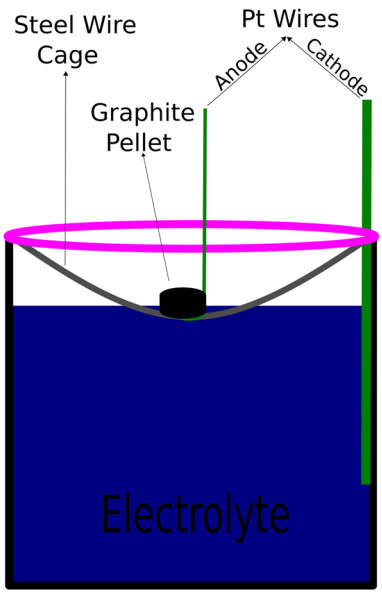


Fig. 1 Schematic drawing of the experimental setup for the exfoliation of powder-like precursors

over the hot plate in order to remove residual moisture, the photoactive layer of P3HT:PCBM solution consisting of 6.5 mg PCBM and 12 mg P3HT in 1 mL chlorobenzene spin-coated over the HTL at 1000 rpm for 30 s. The active layer has also been annealed at 120 °C for 4 min to remove residual moisture. The prepared samples were transferred to a vacuum thermal evaporation system (10^{-5} mbar) for the 100 nm aluminum coating as the cathode electrode. The top Al electrode was deposited through a mask with a periodic rectangular pattern to form a 2×10 mm^2 area cathode with three devices per substrate. The active area for all devices defined by the overlap of ITO and Al electrodes was about 0.1 cm^2. Also, reference samples with only the PEDOT:PSS as HTL have also been prepared with the same method. Figure 2 displays the electrochemical synthesis setup, graphite pellet, stable graphene suspension, and prepared organic solar cell.

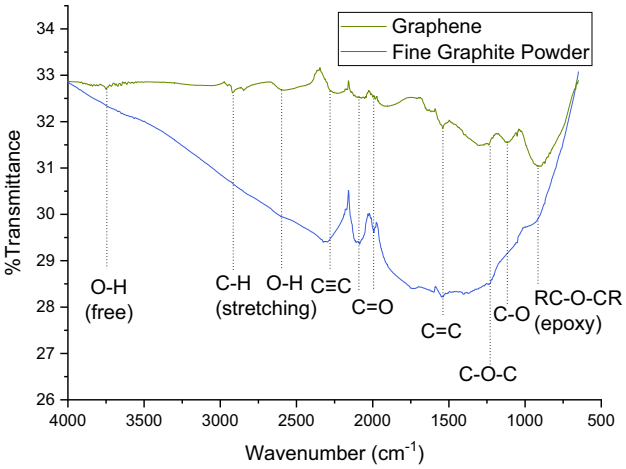


Fig. 3 FT-IR spectrum of electrochemically exfoliated graphene (top) and fine graphite powder (bottom)

3 Results and discussion

The Fourier Transform Infrared (FT-IR) spectroscopic data were obtained using Perkin Elmer Spectrum 100 over the range of 650–4000 cm^{-1}. FTIR spectra of the precursor fine graphite powder and the synthesized graphene can be seen in Fig. 3. FT-IR spectrum is an important tool to identify the bonding vibrations of the sample and the functional groups that have bonded to the surface. FT-IR spectrums of the fine graphite powder precursor and electrochemically synthesized graphene has been investigated in order to determine the surface attached groups on graphene. Main purpose is to determine if any sulfate groups have attached to the graphene surface during the electrochemical process. O–H peaks, free and stretching respectively, at the 3751 cm^{-1} and 2590 cm^{-1} are due to water in the electrolyte [55, 56]. Peaks at 2919, 2227, and 1919 cm^{-1} correspond to C-H (stretching), C≡C, and C = O vibrations [57]. Aromatic C = C peak around ~ 1540 cm^{-1} generally identifies the hexagonal structure and corresponds to the skeletal vibration of the graphitic backbone [58]. The peak at 1118 cm^{-1} depicts the C-O stretching bond at the graphene edge site while peaks at 1236 and 892 cm^{-1} correspond to epoxy groups bound to the surface [59, 60].

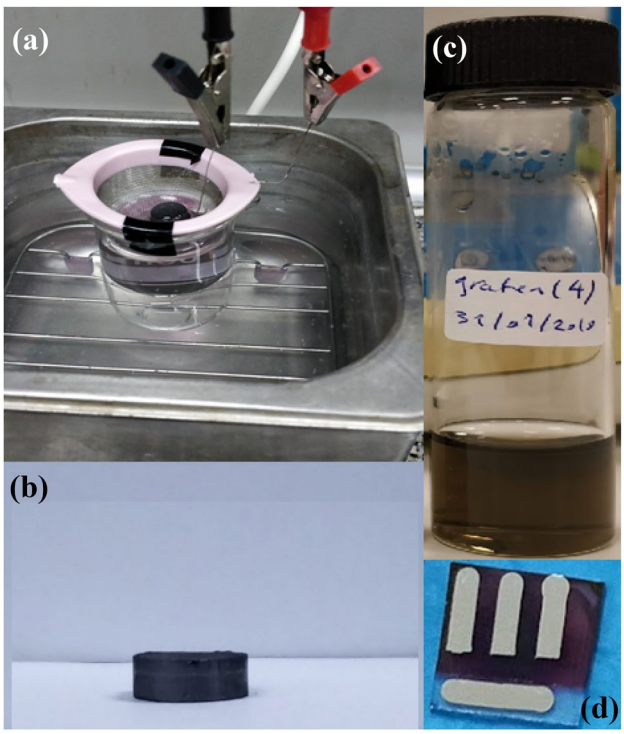


Fig. 2 Electrochemical synthesis setup (**a**), close-up image of graphite pellet (**b**), supernatant (stable graphene suspension in DMF) (**c**), prepared solar cell (**d**)

Raman spectrums have been obtained using a Renishaw inVia Reflex Raman Microscope and Spectrometer with a 532 nm laser. Raman spectroscopy is a non-destructive, fast, and reliable method to investigate the structural and thus, electronic properties of carbon and carbon-related materials. Raman spectra of graphene generally consist of three characteristic peaks such as D, G, and 2D, respectively [61]. The D peak corresponds to the breathing modes of six atom hexagonal rings and appears due to the structural defects in the planar structure. Whereas the G band raises due to in-plane stretching of sp^2 hybridized C atoms, hence it is also a characteristic peak of graphite [37]. D and G peaks in the Raman spectrum correspond to structural defects and the bond stretching of all pairs of sp^2 atoms in both rings and chains, respectively. The ratio of intensities of G and D peaks is a general indicator of structural order and therefore quality of the graphene [62]. Figure 4 shows the Raman

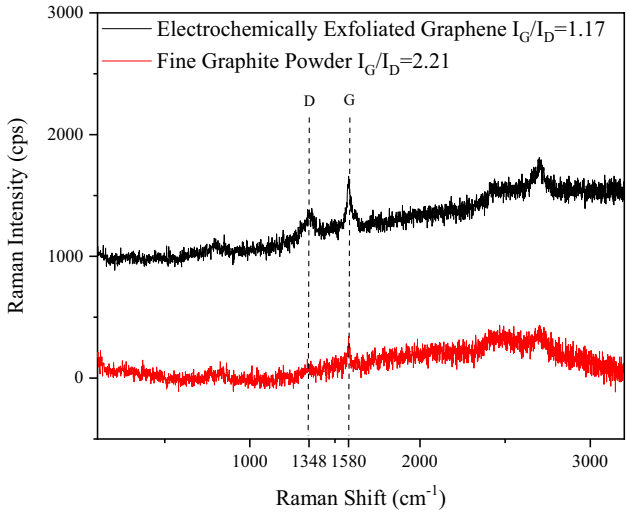


Fig. 4 Raman spectrums of electrochemically produced graphene (top) and fine graphite powder (bottom)

spectrums of both electrochemically exfoliated graphene (top) and fine graphite powder (bottom). It can be seen that the electrochemically produced graphene has a comparable I_G/I_D ratio to the reduction based graphenes [63].

Field Emission Scanning Electron Microscopy is a great technique to investigate micro and/or nano-structure, surface topography, and different phases of the sample. Figure 5 displays FESEM images of the electrochemically produced graphene samples. Figure 5a, b, c show micron-sized graphene sheets while Fig. 5d shows the graphene layer at X10,000, X20,000, X50,000 and X100,000 respectively.

Current density–voltage (J–V) characteristics of the organic solar cells were measured using a computer-controlled Keithley 2400 source meter under illumination. The lighting was provided by Luzchem solar simulator set at 100 mW/cm^2 (AM1.5G) and calibrated using a standard crystalline silicon diode. Short-circuit current I_{sc} (mA), open-circuit voltage V_{oc} (V), and fill-factor (FF) were determined from the J–V curve under illumination to characterize the photovoltaic performance of prepared devices. FF is given by the ratio of the maximum power ($V_{MPP} \times J_{MPP}$) to the product of V_{oc} and J_{sc} (Eq. 1). Power conversion efficiency (PCE) is defined as output electric power (P_{OUT}) to input light power (P_{IN}).

$$FF = \frac{V_{MPP} \times J_{MPP}}{V_{OC} \times J_{SC}} \quad (1)$$

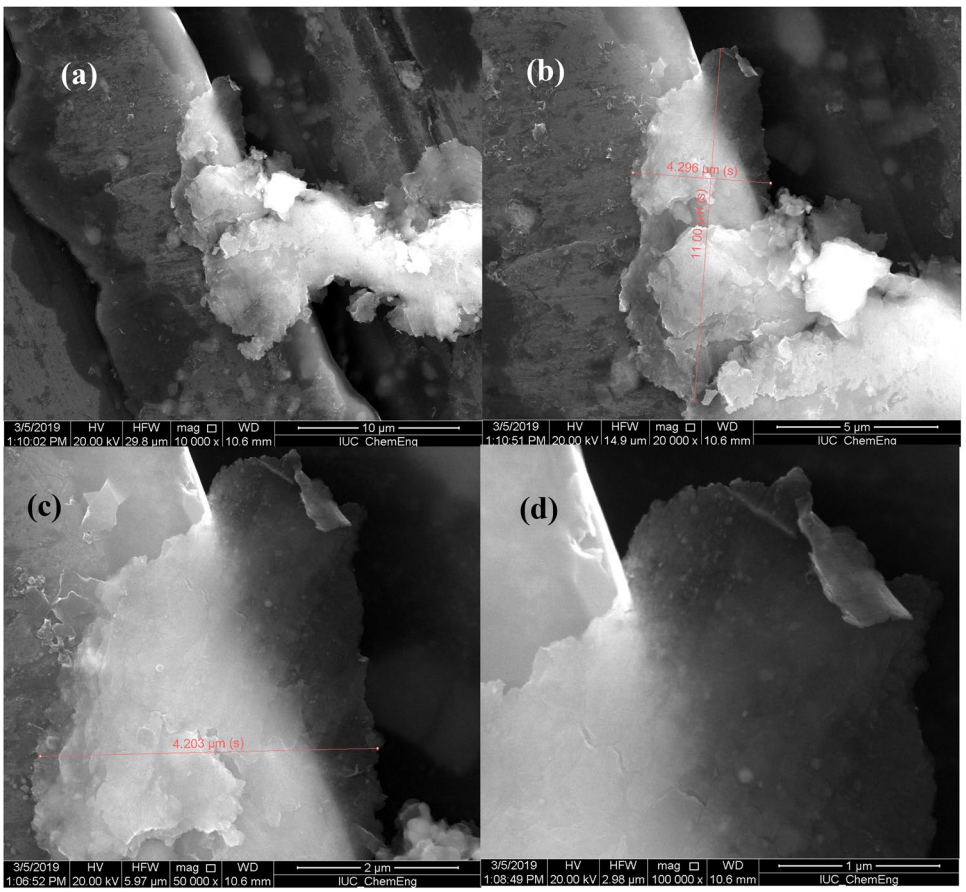


Fig. 5 FE-SEM images of micron sized graphene sheets at (**a**) X10,000, (**b**) X20,000, (**c**) X50,000, and (**d**) X100,000

$$\eta_{AM1.5}(\%) = \left(\frac{P_{out}}{P_{in}}\right) \times 100 = \frac{FF \times V_{OC} \times J_{SC}}{P_{in}} \times 100 \quad (2)$$

The current density–voltage (J–V) characteristics of the organic solar cells prepared with ITO/PEDOT:PSS-Graphene/P3HT:PCBM/Al configuration are shown in Fig. 6. The prepared device without graphene as the reference sample exhibited J_{sc} of 5.6 mA/cm^2, V_{oc} of 575 mV, and an FF of 0.45 was calculated leading to a PCE of 1.5%. Addition of graphene to the PEDOT:PSS layer with a ratio of 5:1 has improved photovoltaic properties significantly such that the device provided a J_{sc} of 8.3 mA/cm^2, V_{oc} of 575 mV, and an FF of 0.52 was calculated leading to a PCE of 2.5% which improved 66.7% compared with the reference device. The photovoltaic parameters of said devices are summarized in Table 1. Compared to previous reports on efficiency increase by the addition of graphene derivatives to the hole transport layer, the effect of incorporating graphene exfoliated by the novel electrochemical exfoliation method to the PEDOT:PSS displays outstanding improvement in the PCE [15, 53, 54].

In order to provide insight into the solar simulation testing methodology, the following histograms have been

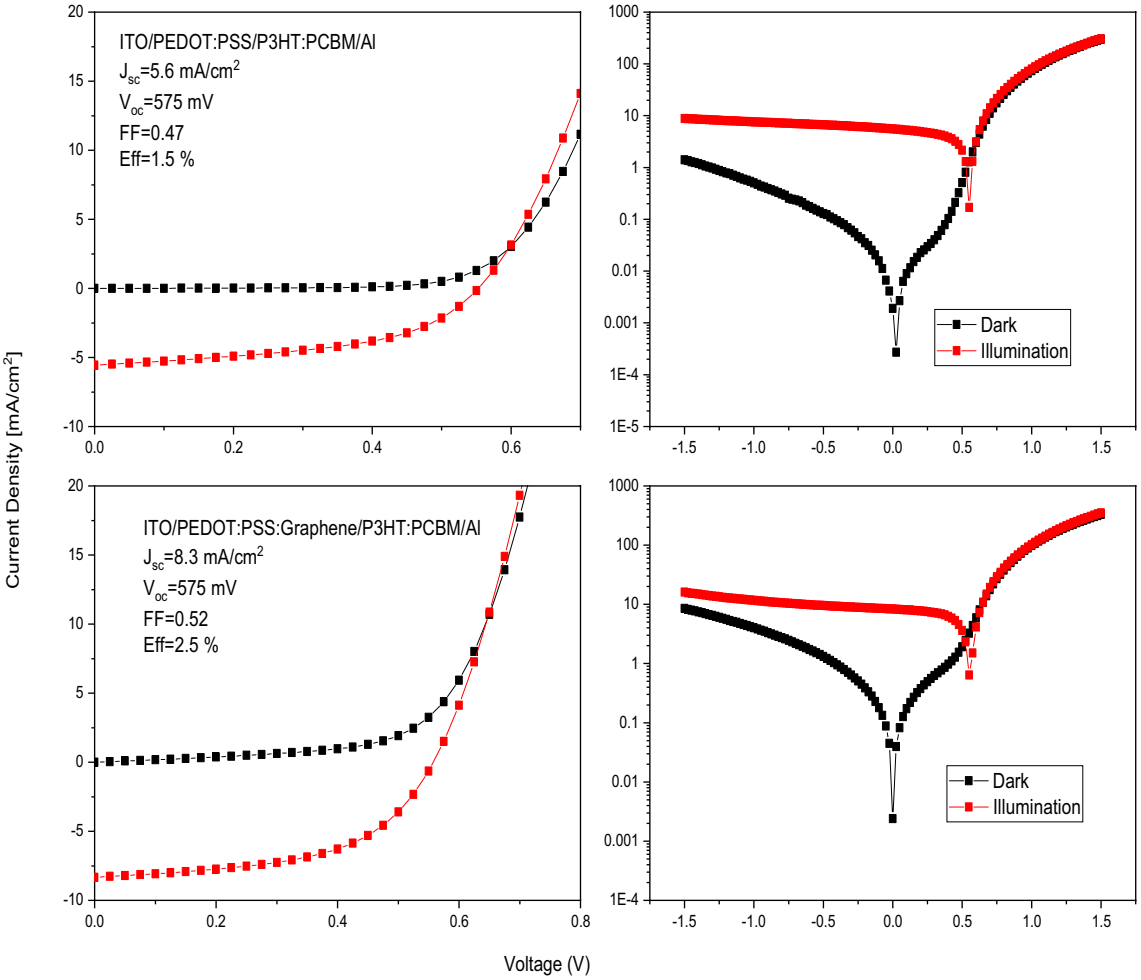


Fig. 6 The current density – voltage characteristics in dark and under the illumination of the organic solar cells with reference PEDOT:PSS and PEDOT:PSS-Graphene

Table 1 The photovoltaic parameters of the prepared OPV devices (15 devices for each condition)

Sample	V_{oc}	J_{sc}	FF (%)	Efficiency (%)	Average Efficiency Values over 15 devices (%)	Standard Deviation (σ)	Improvement
PEDOT:PSS (Ref.)	575 mV	5.6 mA/cm^2	47	1.5	1.27	0.15	–
PEDOT:PSS-Graphene	575 mV	8.3 mA/cm^2	52	2.5	2.27	0.12	66.7%

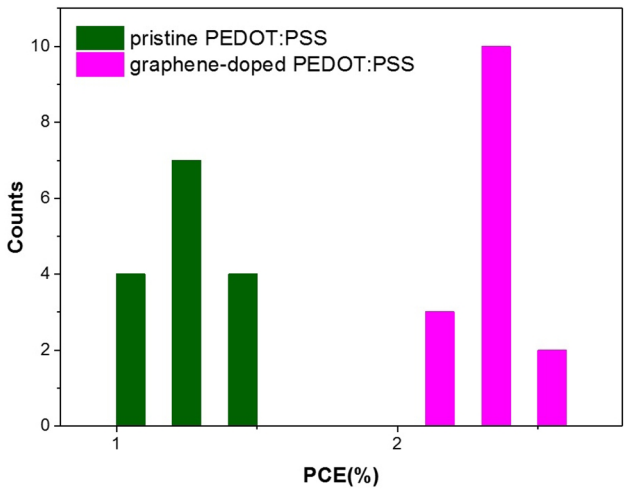


Fig. 7 Result counts vs power conversion efficiency histogram of the reference and the graphene-doped devices

created. Figure 7 displays the result counts vs PCE and Fig. 8 demonstrates the average V_{OC}, J_{SC}, FF, and PCE results with standard deviation for pristine and graphene-doped PEDOT:PSS for 15 devices which show a great reproducibility.

4 Conclusion

To summarize, synthesizing graphene nanosheets with this novel method facilitating steel wire cage and mild sonication has been successful. FT-IR spectra show that there aren't any other surface attached functional groups but the oxygen- and hydrogen-containing ones, which is essential in order to achieve electrochemical exfoliation. Lack of sulfate-containing groups indicates that vacuum filtration and washing procedures have successfully removed the anions from the sample. Raman spectroscopy proves that this method is comparable to the commercial graphene production methods in terms of product quality and the 3D order of the graphite has been broken apart. FESEM images show the micron-sized graphene. Prepared solar cells with graphene as additive vastly outperformed reference (pure) PEDOT:PSS device (%66 increase in efficiency). This efficiency increase is well above the previous reports for graphene derivative HTL additives.

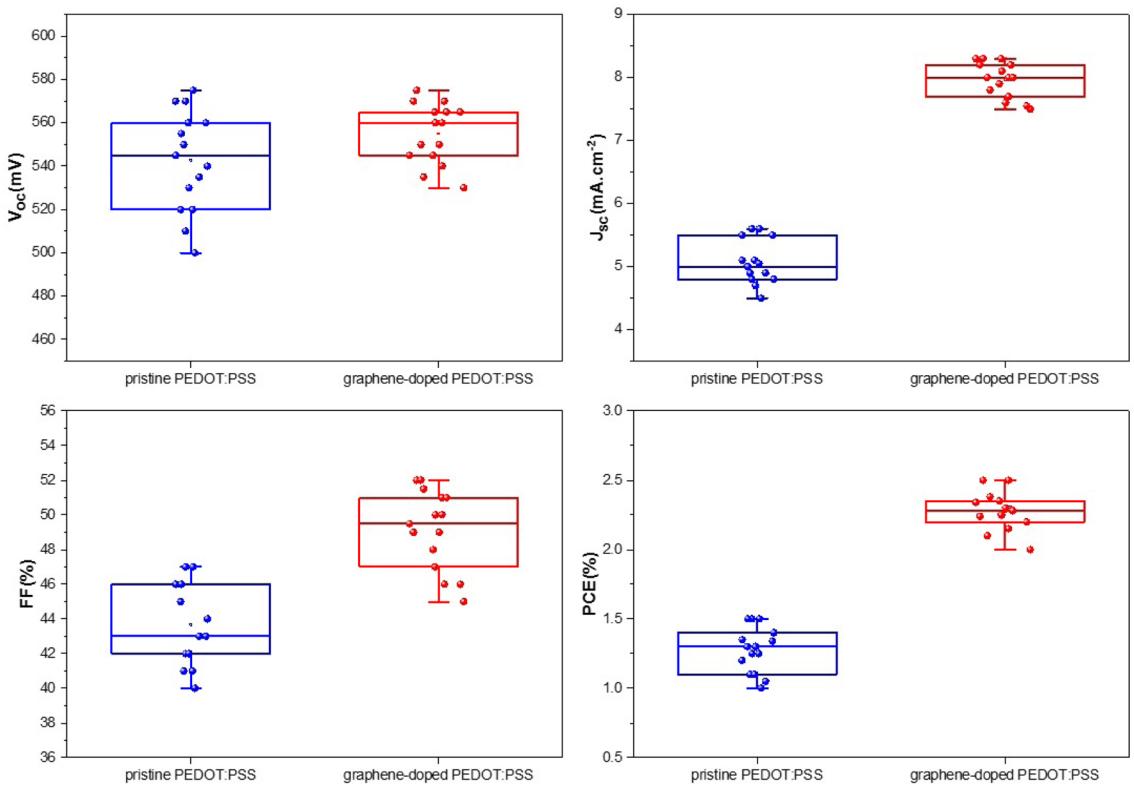


Fig. 8 The average V_{OC}, J_{SC}, FF, and PCE values and their standard deviations for reference and graphene-doped devices

Acknowledgements This study has been funded by the Yıldız Technical University Office of Scientific Research Project No: FYL-2018-3393. The authors would like to express their gratitude to the Yıldız Technical University Office of Scientific Research.

Compliance with ethical standards

Conflict of interest The authors declare that they have no conflict of interest.

References

1. K.S. Novoselov et al., "Electric field in atomically thin carbon films. Science **306**(5696), 666–669 (2004). https://doi.org/10.1126/science.1102896
2. K.S. Novoselov, V.I. FalKo, L. Colombo, P.R. Gellert, M.G. Schwab, K. Kim, A roadmap for graphene. Nature **490**(7419), 192–200 (2012). https://doi.org/10.1038/nature11458
3. A.K. Geim, K.S. Novoselov, The rise of graphene. Nat Mater **6**(3), 183–191 (2007). https://doi.org/10.1038/nmat1849
4. P. Blake et al., Graphene-based liquid crystal device. Nano Lett **8**(6), 1704–1708 (2008). https://doi.org/10.1021/nl080649i
5. C.J. Hung, P. Lin, T.Y. Tseng, High energy density asymmetric pseudocapacitors fabricated by graphene/carbon nanotube/MnO2 plus carbon nanotubes nanocomposites electrode. J Power Sources **259**, 145–153 (2014). https://doi.org/10.1016/j.jpowsour.2014.02.094
6. H.X. Wang, Q. Wang, K.G. Zhou, H.L. Zhang, Graphene in light: Design, synthesis and applications of photo-active graphene and graphene-like materials. Small **9**(8), 1266–1283 (2013). https://doi.org/10.1002/smll.201203040
7. J.P. Llinas et al., Short-channel field-effect transistors with 9-atom and 13-atom wide graphene nanoribbons. Nat Commun **8**(1), 8–13 (2017). https://doi.org/10.1038/s41467-017-00734-x
8. E.B. Bahadir, M.K. Sezgintürk, Applications of graphene in electrochemical sensing and biosensing. TrAC Trends Anal Chem **76**, 1–14 (2016). https://doi.org/10.1016/j.trac.2015.07.008
9. S.H. Hsieh, M.C. Hsu, W.L. Liu, W.J. Chen, Study of Pt catalyst on graphene and its application to fuel cell. Appl Surf Sci **277**, 223–230 (2013). https://doi.org/10.1016/j.apsusc.2013.04.029
10. H.-W. Ha, I.Y. Kim, S.-J. Hwang, R.S. Ruoff, One-pot synthesis of platinum nanoparticles embedded on reduced graphene oxide for oxygen reduction in methanol fuel cells. Electro Chem Solid-State Lett **14**(7), B70 (2011). https://doi.org/10.1149/1.3584092
11. J.G. Radich, P.J. McGinn, P.V. Kamat, Graphene-based composites for electrochemical energy storage. Interface Mag **20**(1), 63–66 (2016). https://doi.org/10.1149/2.f08111if
12. S. Wu, R. Ge, M. Lu, R. Xu, Z. Zhang, Graphene-based nanomaterials for lithium-sulfur battery and sodium-ion battery. Nano Energy **15**, 379–405 (2015). https://doi.org/10.1016/j.nanoen.2015.04.032
13. J.C. Meyer, C.O. Girit, M.F. Crommie, A. Zettl, Imaging and dynamics of light atoms and molecules on graphene. Nature **454**(7202), 319–322 (2008). https://doi.org/10.1038/nature07094
14. C. Zhou, J.A. Szpunar, X. Cui, Synthesis of Ni/graphene nanocomposite for hydrogen storage. ACS Appl Mater Interface **8**(24), 15232–15241 (2016). https://doi.org/10.1021/acsami.6b02607
15. H.S. Dehsari, E.K. Shalamzari, J.N. Gavgani, F.A. Taromi, S. Ghanbary, Efficient preparation of ultralarge graphene oxide using a PEDOT:PSS/GO composite layer as hole transport layer in polymer-based optoelectronic devices. RSC Adv **4**(98), 55067–55076 (2014). https://doi.org/10.1039/c4ra09474c
16. L. Kavan, J.H. Yum, M. Grätzel, Optically transparent cathode for dye-sensitized solar cells based on graphene nanoplatelets. ACS Nano **5**(1), 165–172 (2011). https://doi.org/10.1021/nn102353h
17. B. Paci et al., Stability enhancement of organic photovoltaic devices utilizing partially reduced graphene oxide as the hole transport layer: Nanoscale insight into structural/interfacial properties and aging effects. RSC Adv **5**(129), 106930–106940 (2015). https://doi.org/10.1039/c5ra24010g
18. M. Li et al., Graphene quantum dots as the hole transport layer material for high-performance organic solar cells. Phys Chem Phys **15**(43), 18973–18978 (2013). https://doi.org/10.1039/c3cp53283f
19. A.M. Alexeev, M.D. Barnes, V.K. Nagareddy, M.F. Craciun, C.D. Wright, A simple process for the fabrication of large-area CVD graphene based devices via selective in situ functionalization and patterning. Materials **41**, 1–8 (2017)
20. D.V. Kosynkin et al., Longitudinal unzipping of carbon nanotubes to form graphene nanoribbons. Nature **458**(7240), 872–876 (2009). https://doi.org/10.1038/nature07872
21. P. Wu et al., Few-layered graphene via gas-driven exfoliation for enhanced supercapacitive performance. J Energy Chem **27**(5), 1509–1515 (2018). https://doi.org/10.1016/j.jechem.2017.09.018
22. N.W. Pu, C.A. Wang, Y. Sung, Y.M. Liu, M. Der Ger, Production of few-layer graphene by supercritical CO2 exfoliation of graphite. Mater Lett **63**(23), 1987–1989 (2009). https://doi.org/10.1016/j.matlet.2009.06.031
23. N.M. Huang, H.N. Lim, C.H. Chia, M.A. Yarmo, M.R. Muhamad, Simple room-temperature preparation of high-yield large-area graphene oxide. Int J Nanomed **6**, 3443–3448 (2011). https://doi.org/10.2147/IJN.S26812
24. Y. Si, E.T. Samulski, Synthesis of water soluble graphene. Nano Lett **8**(6), 1679–1682 (2008). https://doi.org/10.1021/nl080604h
25. Y. Xu, H. Bai, G. Lu, C. Li, G. Shi, Y. Xu_et al_G. Shi_Flexible graphene films via the filtration of water soluble non covalent functionalized graphene sheets_JACS_130_2008.pdf. J Am Chem Soc **130**, 5856–5857 (2008)
26. H.R. Kim, S.H. Lee, K.H. Lee, Scalable production of large single-layered graphenes by microwave exfoliation 'in deionized water.' Carbon NY **134**, 431–438 (2018). https://doi.org/10.1016/j.carbon.2018.04.014
27. P. King et al., Scalable production of large quantities of defect-free few-layer graphene by shear exfoliation in liquids. Nat Mater **13**(6), 624–630 (2014). https://doi.org/10.1038/nmat3944
28. J.S.Y. Chia et al., A novel one step synthesis of graphene via sonochemical-assisted solvent exfoliation approach for electrochemical sensing application. Chem Eng J **249**, 270–278 (2014). https://doi.org/10.1016/j.cej.2014.03.081
29. P.E. Resmi, A.L. Palaniayappan, T. Ramachandran, T.G.S. Babu, Electrochemical synthesis of graphene and its application in electrochemical sensing of glucose. Mater Today Proc **5**(8), 16487–16493 (2018). https://doi.org/10.1016/j.matpr.2018.06.001
30. Y.L. Zhong, Z. Tian, G.P. Simon, D. Li, Scalable production of graphene via wet chemistry: progress and challenges. Mater Today **18**(2), 73–78 (2015). https://doi.org/10.1016/j.mattod.2014.08.019
31. J. Wang, K.K. Manga, Q. Bao, K.P. Loh, High-yield synthesis of few-layer graphene flakes through electrochemical expansion of graphite in propylene carbonate electrolyte. J Am Chem Soc **133**(23), 8888–8891 (2011). https://doi.org/10.1021/ja203725d
32. A.T. Najafabadi, E. Gyenge, High-yield graphene production by electrochemical exfoliation of graphite: novel ionic liquid (IL)-acetonitrile electrolyte with low IL content. Carbon NY **71**(58–69), 2014 (2014)
33. A.M. Abdelkader, I.A. Kinloch, R.A.W. Dryfe, Continuous electrochemical exfoliation of micrometer-sized graphene using synergistic ion intercalations and organic solvents. ACS Appl Mater

Interfaces **6**(3), 1632–1639 (2014). https://doi.org/10.1021/am404497n
34. Y.R. Leroux, J.F. Bergamini, S. Ababou, J.C. Le Breton, P. Hapiot, Synthesis of functionalized few-layer graphene through fast electrochemical expansion of graphite. J Electroanal Chem **753**, 42–46 (2015). https://doi.org/10.1016/j.jelechem.2015.06.013
35. G.M. Morales et al., High-quality few layer graphene produced by electrochemical intercalation and microwave-assisted expansion of graphite. Carbon NY **49**(8), 2809–2816 (2011). https://doi.org/10.1016/j.carbon.2011.03.008
36. S. Yang, M.R. Lohe, K. Müllen, X. Feng, New-generation graphene from electrochemical approaches: production and applications. Adv Mater **1**, 6213–6221 (2016). https://doi.org/10.1002/adma.201505326
37. S. Bandi, S. Ravuri, D.R. Peshwe, A.K. Srivastav, Graphene from discharged dry cell battery electrodes. J Hazard Mater **126**(1), 358–369 (2019). https://doi.org/10.1016/j.jhazmat.2018.12.005
38. K. Parvez et al., Exfoliation of graphite into graphene in aqueous solutions of inorganic salts. J Am Chem Soc **136**(16), 6083–6091 (2014). https://doi.org/10.1021/ja5017156
39. M. Coroş et al., Simple and cost-effective synthesis of graphene by electrochemical exfoliation of graphite rods. RSC Adv **6**(4), 2651–2661 (2016). https://doi.org/10.1039/c5ra19277c
40. A.M. Abdelkader, A.J. Cooper, R.A.W. Dryfe, I.A. Kinloch, How to get between the sheets: a review of recent works on the electrochemical exfoliation of graphene materials from bulk graphite. Nanoscale **7**(16), 6944–6956 (2015). https://doi.org/10.1039/c4nr06942k
41. J. Lu, J. Yang, J. Wang, A. Lim, S. Wang, K.P. Loh, One-pot synthesis of fluorescent carbon graphene by the exfoliation of graphite in ionic liquids. ACS Nano **3**(8), 2367–2375 (2009). https://doi.org/10.1021/nn900546b
42. H. Hoppe, N.S. Sariciftci, Morphology of polymer/fullerene bulk heterojunction solar cells. J Mater Chem **16**(1), 45–61 (2006). https://doi.org/10.1039/b510618b
43. T. Mahmoudi, Y. Wang, Y.B. Hahn, Graphene and its derivatives for solar cells application. Nano Energy **47**(February), 51–65 (2018). https://doi.org/10.1016/j.nanoen.2018.02.047
44. V. Shrotriya, G. Li, Y. Yao, C.W. Chu, Y. Yang, Transition metal oxides as the buffer layer for polymer photovoltaic cells. Appl Phys Lett **88**(7), 1–4 (2006). https://doi.org/10.1063/1.2174093
45. M.D. Irwin, D.B. Buchholz, A.W. Hains, R.P.H. Chang, T.J. Marks, p-Type semiconducting nickel oxide as an efficiency-enhancing anode interfacial layer in polymer bulk-heterojunction solar cells. Proc Natl Acad Sci **105**(8), 2783–2787 (2008). https://doi.org/10.1073/pnas.0711990105
46. X. Fan et al., PEDOT:PSS for flexible and stretchable electronics: modifications, strategies, and applications. Adv Sci **6**, 19 (2019). https://doi.org/10.1002/advs.201900813
47. J. Cameron, P.J. Skabara, The damaging effects of the acidity in PEDOT:PSS on semiconductor device performance and solutions based on non-acidic alternatives. Mater Horizons **7**(7), 1759–1772 (2020). https://doi.org/10.1039/c9mh01978b
48. N. Wijeyasinghe et al., Copper(I) Thiocyanate (CuSCN) hole-transport layers processed from aqueous precursor solutions and their application in thin-film transistors and highly efficient organic and organometal halide perovskite solar cells. Adv Funct Mater **27**(35), 1–13 (2017). https://doi.org/10.1002/adfm.201701818
49. J.R. Manders et al., Solution-processed nickel oxide hole transport layers in high efficiency polymer photovoltaic cells. Adv Funct Mater **23**(23), 2993–3001 (2013). https://doi.org/10.1002/adfm.201202269
50. X. Yu, T.J. Marks, A. Facchetti, Metal oxides for optoelectronic applications. Nat Mater **15**(4), 383–396 (2016). https://doi.org/10.1038/nmat4599
51. Y. Lin et al., 17.1% efficient single-junction organic solar cells enabled by n-type doping of the bulk-heterojunction. Adv Sci **7**(7), 1–9 (2020). https://doi.org/10.1002/advs.201903419
52. C.T.G. Smith et al., Graphene oxide hole transport layers for large area, high efficiency organic solar cells. Appl Phys Lett **105**, 7 (2014). https://doi.org/10.1063/1.4893787
53. E. Stratakis, K. Savva, D. Konios, C. Petridis, E. Kymakis, Improving the efficiency of organic photovoltaics by tuning the work function of graphene oxide hole transporting layers. Nanoscale **6**(12), 6925–6931 (2014). https://doi.org/10.1039/c4nr01539h
54. S. Bae, J.U. Lee, H.S. Park, E.H. Jung, J.W. Jung, W.H. Jo, Enhanced performance of polymer solar cells with PSSA-g-PANI/graphene oxide composite as hole transport layer. Sol Energy Mater Sol Cells **130**, 599–604 (2014). https://doi.org/10.1016/j.solmat.2014.08.006
55. J. Oh et al., Graphene oxide porous paper from amine-functionalized poly(glycidyl methacrylate)/graphene oxide core-shell microspheres. J Mater Chem **20**(41), 9200–9204 (2010). https://doi.org/10.1039/c0jm00107d
56. V.K. Singh, M.K. Patra, M. Manoth, G.S. Gowd, S.R. Vadera, N. Kumar, In situ synthesis of graphene oxide and its composites with iron oxide. New Carbon Mater **24**(2), 147–152 (2009). https://doi.org/10.1016/s1872-5805(08)60044-x
57. A. Mir, A. Shukla, Bilayer-rich graphene suspension from electrochemical exfoliation of graphite. Mater Des **156**, 62–70 (2018). https://doi.org/10.1016/j.matdes.2018.06.035
58. R. Bakhshandeh, A. Shafiekhani, Ultrasonic waves and temperature effects on graphene structure fabricated by electrochemical exfoliation method. Mater Chem Phys **212**, 95–102 (2018). https://doi.org/10.1016/j.matchemphys.2018.03.004
59. L.L. Tan, W.J. Ong, S.P. Chai, A.R. Mohamed, Reduced graphene oxide-TiO2 nanocomposite as a promising visible-light-active photocatalyst for the conversion of carbon dioxide. Nanoscale Res Lett **8**(1), 1–9 (2013). https://doi.org/10.1186/1556-276X-8-465
60. K. Zhou, Y. Zhu, X. Yang, X. Jiang, C. Li, Preparation of graphene-TiO2 composites with enhanced photocatalytic activity. New J Chem **35**(2), 353–359 (2011). https://doi.org/10.1039/c0nj00623h
61. A.C. Ferrari, Raman spectroscopy of graphene and graphite: disorder, electron-phonon coupling, doping and nonadiabatic effects. Solid State Commun **143**(1–2), 47–57 (2007). https://doi.org/10.1016/j.ssc.2007.03.052
62. A. Sayah et al., Electrochemical synthesis of polyaniline-exfoliated graphene composite films and their capacitance properties. J Electroanal Chem **818**, 26–34 (2018). https://doi.org/10.1016/j.jelechem.2018.04.016
63. L. Guardia et al., High-throughput production of pristine graphene in an aqueous dispersion assisted by non-ionic surfactants. Carbon NY **49**(5), 1653–1662 (2011). https://doi.org/10.1016/j.carbon.2010.12.049

Publisher's Note Springer Nature remains neutral with regard to jurisdictional claims in published maps and institutional affiliations.